Check for updates

Fs-laser-written erbium-doped double tungstate waveguide laser

ESROM KIFLE,[1] PAVEL LOIKO,[2] CAROLINA ROMERO,[3] JAVIER RODRÍGUEZ VÁZQUEZ DE ALDANA,[3] AIRÁN RÓDENAS,[1,4] VENKATESAN JAMBUNATHAN,[5] VIKTOR ZAKHAROV,[2] ANDREY VENIAMINOV,[2] ANTONIO LUCIANETTI,[5] TOMAS MOCEK,[5] MAGDALENA AGUILÓ,[1] FRANCESC DÍAZ,[1] UWE GRIEBNER,[6] VALENTIN PETROV,[6] AND XAVIER MATEOS[1,*]

[1]*Universitat Rovira i Virgili, Departament Química Física i Inorgànica, Física i Cristal·lografia de Materials i Nanomaterials (FiCMA-FiCNA)-EMaS, Campus Sescelades, E-43007, Tarragona, Spain*
[2]*ITMO University, 49 Kronverkskiy pr., 197101 St. Petersburg, Russia*
[3]*Aplicaciones del Láser y Fotónica, University of Salamanca, 37008 Salamanca, Spain*
[4]*Istituto di Fotonica e Nanotecnologie, Consiglio Nazionale delle Ricerche (IFN-CNR), Piazza Leonardo da Vinci, 32, 20133 Milano, Italy*
[5]*HiLASE Centre, Institute of Physics CAS, Za Radnicí 828, 25241 Dolní Brežany, Czech Republic*
[6]*Max Born Institute for Nonlinear Optics and Short Pulse Spectroscopy, Max-Born-Str. 2a, D-12489 Berlin, Germany*
*xavier.mateos@urv.cat

Abstract: We report on the first erbium (Er^{3+}) doped double tungstate waveguide laser. As a gain material, we studied a monoclinic Er^{3+}:$KLu(WO_4)_2$ crystal. A depressed-index buried channel waveguide formed by a 60 µm-diameter circular cladding was fabricated by 3D femtosecond direct laser writing. The waveguide was characterized by confocal laser microscopy, µ-Raman and µ-luminescence mapping, confirming that the crystallinity of the core is preserved. The waveguide laser, diode pumped at 981 nm, generated 8.9 mW at 1533.6 nm with a slope efficiency of 20.9% in the continuous-wave regime. The laser polarization was linear ($E \parallel N_m$). The laser threshold was at 93 mW of absorbed pump power.

1. Introduction

The Erbium (Er^{3+}) ion is known for its laser emission around 1.5 µm wavelength due to the $^4I_{13/2} \rightarrow {}^4I_{15/2}$ transition [1]. This emission is eye-safe and it corresponds to one of the transparency windows of atmosphere and silica fibers. Er-doped silica fiber lasers and amplifiers are the workhorse in telecommunication. Furthermore, Er lasers are used in free-space communications, range-finding (LIDAR), navigation and environmental sensing. Continuous-wave (CW) and pulsed waveguide Er lasers are of practical importance for integrated optics [2] as well. Various methods have been implemented for the fabrication of Er waveguides for lasers and amplifiers, e.g., ion diffusion [3], ion exchange [4], reactive co-sputtering [5], pulsed laser deposition [6], liquid phase epitaxy [7], femtosecond direct laser writing (fs-DLW) [8], etc.

The Er^{3+} ion (electronic configuration: [Xe]$4f^{11}$) possesses a complex energy levels scheme with multiple resonant energy-differences between multiplets [9]. This determines various possible transfer processes of electronic excitation, e.g., energy-transfer upconversion (ETU), excited-state absorption (ESA) or cross-relaxation (CR) [9,10]. For the 1.5 µm laser emission, these processes are parasitic limiting the laser efficiency and causing unwanted heat loading. Thus, the selection of a proper Er^{3+} doping concentration as well as pumping scheme is critical.

The most well-known scheme is (Er^{3+},Yb^{3+}) codoping with the Yb^{3+} ion serving as a sensitizer and providing strong absorption at 0.98 µm (range of emission from InGaAs laser

diodes). For certain materials like phosphate glasses, this scheme is rather efficient [11,12]. In-band pumping of Er^{3+} ions at ~1.5 µm (directly to the $^4I_{13/2}$ upper laser level) has proven its potential for power-scalable crystalline lasers, e.g., $Er:Y_3Al_5O_{12}$ [13], but the suitable pump sources are not widely spread and expensive. Pumping of singly Er^{3+}-doped crystals at 0.98 µm (to the $^4I_{11/2}$ state) can be a cheap alternative [14] although the optical-to-optical efficiency of such lasers is limited by the low $^4I_{15/2} \rightarrow {}^4I_{11/2}$ absorption.

Among the hosts for laser-active rare-earth ions (RE^{3+}), monoclinic double tungstates (MDTs) having a chemical formula $KRE(WO_4)_2$ where RE = Gd, Y or Lu, have been extensively studied. These crystals feature high transition cross-sections with polarized light, weak non-radiative relaxation, long RE^{3+}-RE^{3+} distances and acceptance of high RE^{3+} doping concentrations [15]. Efficient MDT lasers based on Nd^{3+} and Yb^{3+} (at ~1 µm), Tm^{3+} and Ho^{3+} (at ~2 µm) doping have been reported [16–18]. Moreover, efficient MDT waveguide (WG) lasers have also been demonstrated [19,20]. Typically, they are based on thin films grown by liquid phase epitaxy (LPE) [21] and (optionally) microstructured by ion etching.

However, there are only few studies devoted to Er:MDT lasers [14,22,23] and there are no reports on Er:MDT WG lasers. An $Er,Yb:KY(WO_4)_2$ laser generated only 2.8 mW at 1.54 µm with a slope efficiency η of ~1% [22]. In-band pumping of Er:MDTs at 1.52 µm has been also realized, while still with limited output power, e.g., 110 mW at 1.609 µm with $\eta = 40\%$ for $Er:KY(WO_4)_2$ [23]. Very recently, direct diode-pumping of singly-doped $Er:KLu(WO_4)_2$ crystal was demonstrated reaching 268 mW of CW output at 1.610 µm with $\eta = 30\%$ [14]. Note that tetragonal double tungstates, $NaRE(WO_4)_2$, have been considered as hosts for Er^{3+} doping as well [24].

Regarding Er:MDT WGs, previous studies focused on their fabrication and Er^{3+} spectroscopy [7,25–27]. Bolaños *et al.* reported on the growth of "mixed" $Er:KY_{1-x-y}Gd_xLu_y(WO_4)_2$ layers on undoped $KY(WO_4)_2$ substrates by LPE [25]. Upconversion luminescence of LPE-grown $Er,Yb:KY(WO_4)_2$ thin films was studied in [26]. Recently, the gain in 0.98 µm-pumped singly Er^{3+}-doped $KGd_{1-x}Lu_y(WO_4)_2$ channel WGs was studied. A relative internal gain (signal enhancement minus absorption) of 12 ± 5 dB/cm at 1.535 µm, ESA spectra and ETU micro-parameters were determined [7]. Kurilchik *et al.* reported on the growth, spectroscopy and "bulk" laser operation of $Er,Yb:KGd_{1-x}Y_x(WO_4)_2$ LPE-grown thin films. Under in-band pumping in non-waveguiding geometry, 16 mW of CW output were achieved at 1.606 µm with $\eta = 64\%$ [27].

In the present work, we demonstrate the first Er-doped MDT WG laser. A singly Er^{3+} doped bulk MDT crystal is diode-pumped at ~0.98 µm (to the $^4I_{11/2}$ state). The waveguide was fabricated by 3D femtosecond direct laser writing (fs-DLW). Fs-DLW is a powerful tool to produce active microstructures in transparent dielectric materials [28–30]. It has been previously used to fabricate waveguides in Er^{3+},Yb^{3+}-codoped glasses applied for amplifiers [31] and lasers [8,32,33]. Fs-DLW MDT WG lasers based on Yb^{3+} and Tm^{3+} ions have been reported recently [34,35].

Fs-DLW of active waveguides in RE^{3+}-doped low-symmetry crystals like MDTs in the geometries of type II or depressed cladding (with a negative refractive index change) [30] is expected to benefit from the anisotropy of spectroscopic properties of RE^{3+} ions in crystals and better thermal and thermo-mechanical properties of the host matrix, as compared to glasses. Note that it is typically not possible to produce type I WGs (with a positive refractive index change) in such crystals contrary to glasses [30].

2. Experimental

2.1 Laser crystal

As a laser crystal, we used $Er:KLu(WO_4)_2$ (below, it is denoted shortly as Er:KLuW). The Er^{3+} doping concentration was 1 at. % ($N_{Er} = 0.64 \times 10^{20}$ cm^{-3}). The crystal was grown by the Top-Seeded Solution Growth (TSSG) Slow-Cooling method using $K_2W_2O_7$ as a solvent and a

[010]-oriented seed [15]. A rectangular sample was cut for light propagation along the N_g optical indicatrix axis. It had a length t of 3 mm and an aperture of $3(N_m) \times 3(N_p)$ mm^2. Both $N_m \times N_p$ faces, as well as one of the lateral side faces were polished to laser quality and remained uncoated.

2.2 Waveguide fabrication

The depressed-index buried channel WG was fabricated in the bulk Er:KLuW sample by fs-DLW [35], Fig. 1. For writing, we used a Ti:Sapphire regenerative amplifier (Spitfire, Spectra Physics) operating at 795 nm and emitting 120 fs pulses at a repetition rate of 1 kHz. As focusing optics, a 40 × (N.A. = 0.65) microscope objective was used. The incident pulse energy on the crystal was 74 nJ, only a small fraction of the Spitfire output energy (~1 mJ) that was reduced by using a set of a half-wave plate, a linear polarizer and a calibrated neutral density (ND) filter. The fs-DLW was performed through the polished lateral side face of the sample. The crystal was scanned at a speed of 400 μm/s along the N_g-axis producing damage tracks through the whole length of the sample. The damage tracks reached both sample end-facets but no surface damage was observed. As a result, the end-facets were not repolished after fs-DLW. The polarization of the fs laser corresponded to $E \parallel N_m$ in the crystal, so that it was perpendicular to the scanning direction, see Ref [36]. for reasoning.

The channel WG consisted of a 60 μm diameter core and a ring-shaped cladding formed by fs laser damage tracks. The axis of the WG was located 120 μm beneath the crystal surface. The separation between adjacent tracks along the perimeter of the core was ~2 μm. The WG was written along the entire crystal length (3 mm). The refractive index of KLuW n_m is 2.024 (at 1.534 μm, for $E \parallel N_m$) [37]. According to our previous study [36], the decrease of the refractive index in the cladding region Δn is ~6×10^{-4}.
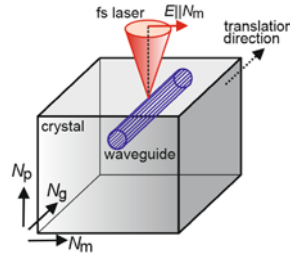

Fig. 1. Scheme of the 3D femtosecond direct laser writing of the channel waveguide in Er:KLuW.

2.3 Waveguide characterization

The fs-DLW WG was studied using a confocal laser microscope (LSM 710, Carl Zeiss) equipped with a set of a polarizer and an analyzer, a blue GaN laser ($\lambda = 405$ nm) and an Ar$^+$ ion laser ($\lambda = 488$ nm).

For μ-Raman and μ-luminescence mapping, we used a Renishaw inVia Reflex confocal Raman microscope with a He-Ne laser ($\lambda = 632.8$ nm) and an Ar$^+$ ion laser ($\lambda = 514$ nm), respectively. It was equipped with a 50 × Leica objective and a set of polarizers and an analyzer. The spatial resolution was 0.4 μm.

The luminescence spectra were measured using OSAs (model AQ6373 for visible and model AQ6375B for near-IR, Yokogawa) and a Glan-Taylor polarizer. The VBG-stabilized InGaAs laser diode at 981 nm (described in Section 2.3) was applied as excitation source. The decay curves were measured under quasi-CW excitation using a 2 GHz digital oscilloscope (Tektronix DPO5204B) and an InGaAs photodiode.

2.4 Laser set-up

The Er:KLuW sample containing the fs-DLW WG was mounted on an Al holder between conventional cavity mirrors. The passively-cooled holder was kept at room temperature (RT, 293 K) and no noticeable change of the temperature was detected during the laser operation. The laser cavity consisted of a flat pump mirror (PM) coated for high transmission (HT) at 0.98 μm and for high-reflection (HR) at 1.52–1.70 μm and a flat output coupler (OC) having a transmission of $T_{OC} = 1\%$, 2% or 5% at the laser wavelength. Both PM and OC were placed as close as possible to the WG end-facets while no index-matching liquid was used.
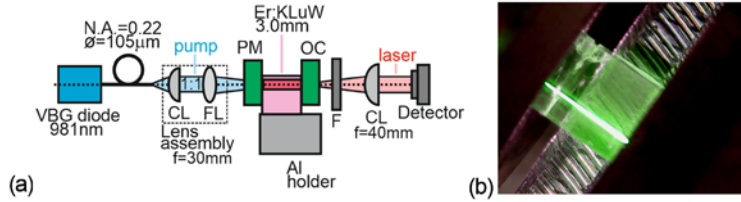

Fig. 2. (a) Laser set-up: CL – collimating lenses, FL -focusing lens, PM – pump mirror, OC – output coupler, F – filter; (b) photograph of the green upconversion from the pumped fs-DLW Er:KLuW waveguide.

The WG was pumped by an InGaAs laser diode (fiber core diameter: 105 μm, numerical aperture: 0.22). Its unpolarized emission at 981 nm was stabilized by a volume Bragg grating (emission bandwidth: 0.7 nm). The fiber output was collimated and focused into the crystal by a lens assembly (1:1 imaging ratio, focal length f = 30 mm). The pump spot size on the input facet of the WG $2w_p$ was 105 μm. The pump radiation coupling efficiency was estimated from the geometrical overlap of the focused pump beam and the WG core as $29 \pm 2\%$ (accounting for the Fresnel losses). The measured pump absorption under lasing conditions $\eta_{abs,L}$ was $9.5 \pm 0.5\%$.

The laser output was filtered from the residual pump with a long-pass dielectric filter and collimated with an aspherical uncoated plano-convex lens (f = 40 mm). The output power was measured with a power meter (Ophir Nova P/N 1Z01500), the emission spectrum was recorded using an optical spectrum analyzer (OSA, Yokogawa, model AQ6375B) and the beam profile was captured using a near-IR camera (FIND-R-SCOPE model 85726). The calibration of the camera was performed using a 1951 USAF resolution test target (Thorlabs, model R1DS1) placed at the position of the output facet of the WG and illuminated by the pump beam.

The scheme of the laser set-up is shown in Fig. 2(a). The Er:KLuW WG under lasing conditions emitted bright green Er^{3+} upconversion luminescence (the $^2H_{11/2} + {}^4S_{3/2} \rightarrow {}^4I_{15/2}$ transition). The greenish luminescence in Fig. 2(b) indicates the pump channel.

3. Results and discussion

3.1 Confocal microscopy study

At first, we studied the fs-DLW Er:KLuW WG by confocal microscopy, see Fig. 3. The measurements were done in transmission with polarized light at $\lambda = 405$ nm. When looking at one of the polished end-facets, a dark ring is formed by vertically extended (1.5...2 × 5...8 μm^2 along horizontal and vertical directions, respectively) damage tracks, representing the WG cladding, Fig. 3(a). The WG core appears to be darker than the bulk region because of attenuation of light passing through the core and cladding. No cracks in the inner core and surrounding bulk regions are visible.

When looking from above on the central part of the WG (along the direction of propagation of the writing fs laser), a dark barrel with a net-like structure surrounded by a bright bulk area is observed, Fig. 3(c). The selected sample scanning speed (400 μm/s)

ensures the continuity of the damage lines along the sample as clearly seen in Fig. 3(c). On the other hand, the use of a smaller scanning speed is detrimental for the WG performance provided that a more severe damage will be induced increasing propagation loss, and the cumulative effects of the stress may distort the mode profile. The inhomogeneity in the damage tracks that can be seen in Fig. 3(c) is related to a minor defect in the motion of the XYZ stage.
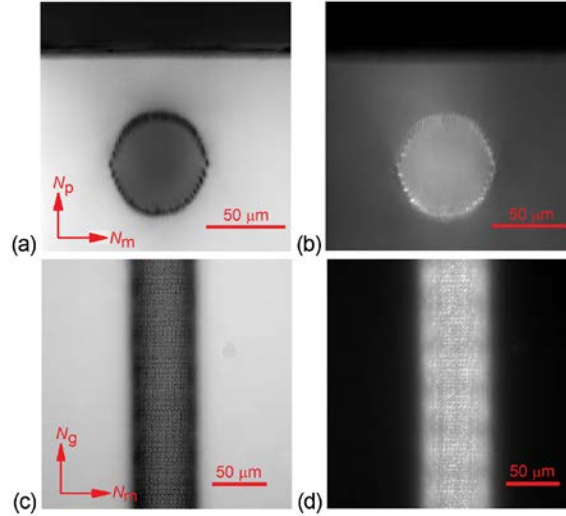

Fig. 3. Transmission-mode confocal microscope images of the fs-DLW Er:KLuW waveguide: (a,b) end-facet view, (c,d) top view. (a,c) polarized (P) light, (a) P $\parallel N_p$, (c) P $\parallel N_g$, $\lambda = 405$ nm, (b,d) with crossed polarizer (P) and analyzer (A), (b) P $\parallel N_p$, A $\parallel N_m$, (d) P $\parallel N_g$, A $\parallel N_m$, $\lambda = 488$ nm.

To reveal the effect of fs-DLW on the induced birefringence of the WG, it was further studied with crossed polarizers. Monoclinic KLuW is an optically biaxial crystal [15]. If placed between two crossed polarizers oriented along two orthogonal optical indicatrix axes, it will show a dark field in transmission. The latter is seen in the bulk regions in Fig. 3(b) (end-facet view) and Fig. 3(d) (top view). Fs-DLW induces a modification of the structure and the stress field leading to a local alteration of the optical indicatrix via the photo-elastic effect. Light is therefore transmitted through the crossed polarizers due to an additional phase shift within the crystal, as shown in Figs. 3(b) and 3(d).

3.2 µ-Raman mapping

µ-Raman mapping is a sensitive method to monitor the alteration of crystallinity (degree of structural order, i.e., the lack of lattice defects, imperfections and structure disorder) of samples intended for fs-DLW [38].

The Raman spectra were measured in the $g(mm)g$ geometry focusing on the most intense internal mode of KLuW appearing at ~908 cm^{-1}. Its peak intensity, peak position and width were monitored. This mode is assigned as v(W–O)/v_1 and related to the W–O stretching vibrations of the [WO$_6$] octahedra in the KLuW structure [15].
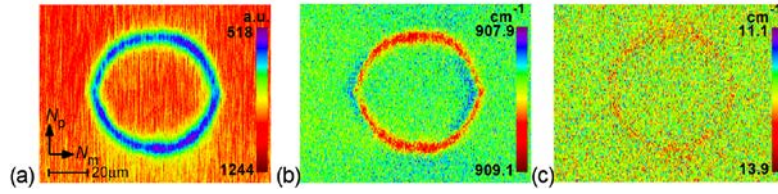
Fig. 4. µ-Raman mapping of the polished end-facet of a fs-DLW Er:KLuW waveguide, $g(mm)g$ geometry, monitoring the ~908 cm^{-1} Raman peak: (a) peak Raman intensity, (b) peak position, (c) peak width, λ_{exc} = 632.8 nm.

The results of the µ-Raman mapping of one of the WG end-facets are shown in Fig. 4. In the WG core region, the crystalline quality of the material is preserved, as indicated by the unchanged Raman response with respect to the bulk crystal. In the cladding, the peak intensity of the studied Raman band decreased, the peak position shifted to higher frequencies (to 909.1 cm^{-1}), and a slight broadening of the peak was observed, indicating a reduction of the structural order and appearing stresses [38–41]. Note that as it was shown in Section 3.1, no macroscopic crystal damage was detected.

3.3 µ-luminescence mapping

µ-luminescence mapping allows to analyze the effect of fs-DLW on the emission properties of active ions.
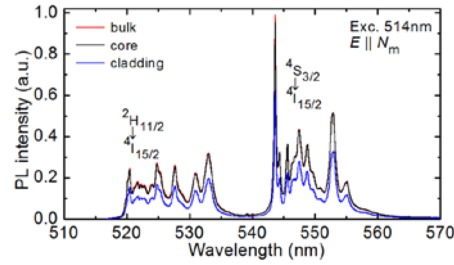

Fig. 5. Spectra of the Er^{3+} luminescence due to the $^2H_{11/2}$ + $^4S_{3/2}$ → $^4I_{15/2}$ transitions measured from the bulk, core and cladding regions of the end-facet of a fs-DLW Er:KLuW waveguide, λ_{exc} = 514 nm, excitation / detection light polarization is $E \parallel N_m$.

The luminescence spectra of Er^{3+} corresponding to the $^2H_{11/2}$ + $^4S_{3/2}$ → $^4I_{15/2}$ transition (corresponding to the green spectral range) measured from the bulk, WG core and WG cladding regions are shown in Fig. 5. The excitation / detection light polarization is $E \parallel N_m$. The shape of the spectra for all three studied areas is almost the same. The emission intensity decreases when going from the bulk and the WG core to the WG cladding.

To trace such changes, we selected a well-resolved peak at 552.8 nm due to the Stark-to-Stark transition within the $^4S_{3/2}$ → $^4I_{15/2}$ emission band. The peak intensity, peak position and peak width were analyzed, see Fig. 6. In the WG core region, no notable change of the luminescence response is detected with respect to the bulk crystal. In the WG cladding region, the luminescence intensity is suppressed and the Stark-to-Stark emission peak is broadened experiencing a red-shift. The former effect is attributed to the luminescence quenching by fs-DLW-induced color centers (structure imperfections) and the two latter effects – to the slightly modified crystal-field arising from lattice disorder in the WG cladding [38]. In Figs. 6(b) and 6(c), a weak horizontal area extending over the WG core is observed where the emission properties are weakly altered. It is attributed to the so-called anisotropic stress fields induced by fs-DLW [41].
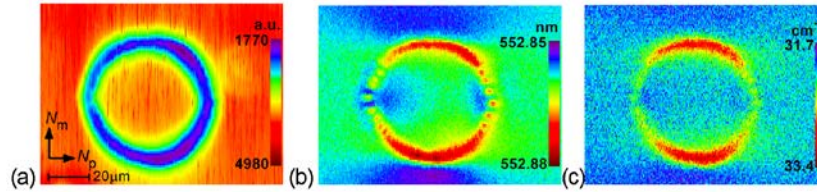
Fig. 6. μ-luminescence mapping of the polished end-facet of a fs-DLW Er:KLuW waveguide on the $^4S_{3/2} \rightarrow {}^4I_{15/2}$ Er^{3+} transition: (a) luminescence intensity, (b) peak position, (c) peak width, λ_{exc} = 514 nm, λ_{lum} = 552.8 nm, excitation / detection light polarization is $E \parallel N_m$.

3.4 The Er^{3+} $^4I_{13/2} \rightarrow {}^4I_{15/2}$ transition at ~1.5 µm

Prior to the laser experiments, we also characterized the ~1.5 µm emission of Er^{3+} from the WG core according to the $^4I_{13/2} \rightarrow {}^4I_{15/2}$ transition. The collecting fiber of the OSA was placed next to the output facet of the WG which was pumped at ~981 nm by unpolarized light. The polarized luminescence spectra are shown in Fig. 7(a). They are strongly polarized; the maximum intensity corresponds to $E \parallel N_m$. The local peak in the emission spectra is at 1535 nm. The corresponding stimulated-emission cross-section σ_{SE} is 3.0×10^{-20} cm^{-2} [14].
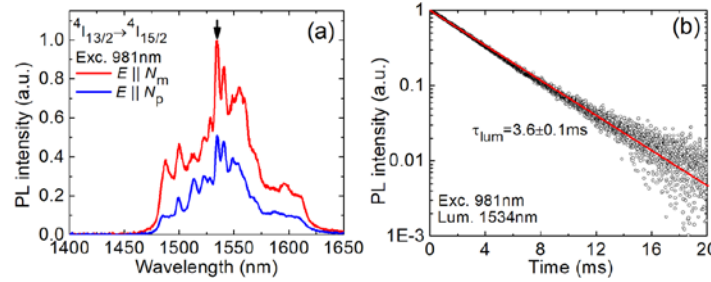

Fig. 7. $^4I_{13/2} \rightarrow {}^4I_{15/2}$ emission from the fs-DLW Er:KLuW waveguide: (a) photo luminescence (PL) spectra for light polarizations $E \parallel N_m$ and $E \parallel N_p$, *arrow* indicates the laser wavelength; (b) luminescence decay curve: *symbols* – experimental data, *line* – single-exponential fit, λ_{exc} = 981 nm, λ_{lum} = 1534 nm.

The luminescence decay curve at 1.534 µm is shown in Fig. 7(b). It is clearly single-exponential with a characteristic decay time τ_{lum} of 3.6 ± 0.1 ms. This value is close to that measured for a bulk Er:KLuW crystal [14]. The single-exponential decay confirms the presence of a single type of site for Er^{3+} ions (Lu^{3+} site, VIII-fold O^{2-} coordination, C$_2$ symmetry) [15]. Thus, fs-DLW does not affect the site symmetry for Er^{3+} ions in the WG core region.

3.5 Laser operation

Laser operation was achieved with the fs-DLW Er:KLuW WG using all applied OCs (1%-5%). The laser output was linearly polarized ($E \parallel N_m$), naturally selected by anisotropy of the gain [14]. No damage of the WG was observed under laser operation up to an incident pump power of at least 5.2 W.

The input-output dependences are shown in Fig. 8(a). The maximum output power corresponded to T_{OC} = 5%, namely 8.9 mW at 1533.6 nm with a slope efficiency η of 20.9% (with respect to the absorbed pump power P_{abs}). The laser threshold was at P_{abs} = 93 mW. For smaller output coupling, the laser output deteriorated: η = 10.6% and 2.1% for T_{OC} = 2% and 1%, respectively. For all studied OCs, the input-output dependences were linear showing no detrimental thermal effects. Due to the small number of available OCs, we were not able to perform the Caird analysis (a plot of inverse of the slope efficiency *vs.* inverse of the output-coupling losses) [42]. The propagation losses in similar fs-DLW circular 3 at.% Tm:KLuW WGs were recently estimated by us from the Caird analysis to be about 1.4 ± 0.5 dB/cm at

1.84 µm [35] while the exact value is expected to vary slightly with the RE^{3+} ion and the doping concentration.

Typical spectra of the fs-DLW Er:KLuW WG laser are shown in Fig. 8(b). The laser wavelength λ_L experienced a slight blue-shift with increasing T_{OC}, from 1535.2 to 1533.6 nm in agreement with the quasi-three-level nature of the Er^{3+} laser for this transition. The weak dependence of the laser wavelength on the output coupling is explained by relatively high intracavity losses of the WG laser leading to high inversion ratios $\beta = N_2(^4I_{13/2})/N_{Er}$. According to the gain spectra of Er^{3+} in KLuW for light polarization $E \parallel N_m$ [14], the local peak at ~1535 nm dominates in the spectra for very high $\beta > 0.55$ (strongly bleached WG). The latter agrees with the determined pump absorption under lasing conditions $\eta_{abs,L}$ (Section 2.4) which is much smaller than the small-signal pump absorption calculated from the spectroscopic data, $\eta_{abs,0} = 1 - \exp(-\sigma^p_{abs}N_{Er}t) = 20.6\%$ (assuming no ground-state bleaching). Here, $\sigma^p_{abs} = 1.2 \times 10^{-20}$ cm^2 is the absorption cross-section at the pump wavelength (averaged for $E \parallel N_m$ and $E \parallel N_p$ polarizations) [14].

The spatial profile of the laser output beam was measured in the far-field. The equivalent size of the mode at the output facet of the WG was determined using far-field beam profiles obtained with a resolution test target placed at the position of the WG output facet. The results are shown in Fig. 8(c) for $T_{OC} = 5\%$ (the mode size was nearly unchanged for all studied OCs). The mode is nearly-spherical and the intensity profiles in the directions of the N_m and N_p axes are well fitted to a Gaussian distribution. The resulting mode sizes $2w_L$ are 48.2 µm and 49.4 µm, respectively. Thus, the mode is well-confined within the WG core.
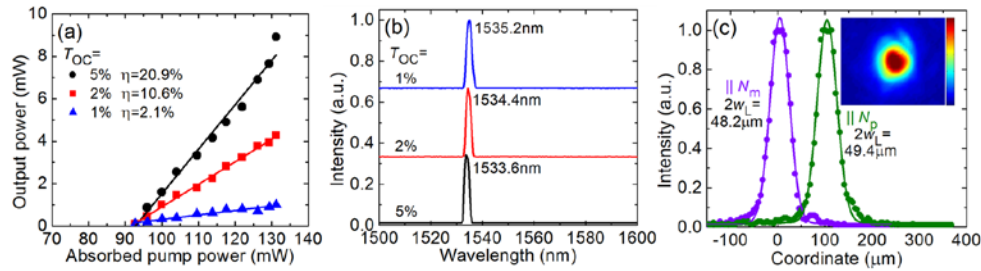

Fig. 8. Diode-pumped fs-DLW Er:KLuW waveguide laser: (a) input-output dependences, η – slope efficiency; (b) typical laser emission spectra measured at $P_{abs} = 116$ mW; (c) calibrated spatial profiles of the laser mode corresponding to the output facet of the WG: *symbols* – experimental data, *curves* – their Gaussian fits, *inset* – 2D profile, $T_{OC} = 5\%$, $P_{abs} = 116$ mW.

Table 1. Output Characteristics of Er fs-DLW Waveguide Lasers Reported So Far

Active material	λ_p, nm	P_{th}, mW	P_{out}, mW	λ_L, nm	η, %	Ref.
Er^{3+},Yb^{3+}-codoped glass						
phosphate	976&980	142	80	1535	21.5[inc]	[43]
phosphate	976&980	90	23	1560	6.6[inc]	[32]
phosphate	975	330	1.7	1533	2[inc]	[8]
oxyfluoride-silicate	980&1480	350	0.03	1536	0.01[inc]	[44]
La-phosphate	976	350	5	1535	~2[inc]	[33]
La-phosphate	976	21.6	112	1535	38.3[abs]	[45]
Er^{3+}-doped crystal						
KLu(WO$_4$)$_2$	981	93	8.9	1534	20.9[abs]	This work
LiLuF$_4$	974	1150	10	553	3[inc]	[46]

In Table 1, we compared the output characteristics of the fs-DLW Er WG lasers reported so far [8,32,33,43–46]. To date, most of the studies focused on Er^{3+},Yb^{3+}-codoped glasses, namely phosphate, La-phosphate and oxyfluoride-silicate. The maximum output power was

achieved in [45] using a 2 wt.% Er_2O_3, 4 wt% Yb_2O_3 doped $P_2O_5 - La_2O_3 - Al_2O_3 - K_2O$ glass and diode-pumping at 976 nm, namely 112 mW at 1535 nm with a maximum $\eta = 38.3\%$ (with respect to P_{abs}). Single-longitudinal-mode (SLM) operation was obtained by fiber Bragg grating mirrors. The use of other glass compositions typically led to lower output powers and slope efficiencies [8,33,44].

This work represents the first ~1.5 µm fs-DLW Er crystalline WG laser. A previous study on fs-DLW waveguides in $Er:LiLuF_4$ crystal focused on upconversion laser emission at 553 nm ($^4S_{3/2} \rightarrow {}^4I_{15/2}$ transition) [46].

4. Conclusion

To conclude, we report on the first ~1.5 µm fs-DLW erbium crystalline waveguide laser, as well as the first erbium-doped double tungstate waveguide laser. It is based on a monoclinic singly Er^{3+}-doped $KLu(WO_4)_2$ crystal diode-pumped at ~0.98 µm (to the $^4I_{11/2}$ state). Strong polarization-anisotropy of transition cross-sections for Er^{3+}-doped MDTs promotes the possibility of direct diode-pumping of singly Er^{3+}-doped crystals. In addition, 3D fs-DLW allowed us to fabricate channel waveguides with well-preserved crystallinity of the core, as confirmed by µ-Raman and µ-luminescence mapping.

The designed waveguide laser generates 8.9 mW of CW output at 1533.6 nm (a wavelength corresponding to the telecom C-band) with a slope efficiency of >20%, linear laser polarization ($E \parallel N_m$) and nearly-Gaussian output beam. The laser threshold is as low as 93 mW of absorbed pump power. We believe that it is possible to improve the WG laser performance by a proper combination of Er^{3+} concentration and output coupling. In-band pumping of the WG laser can lead to even higher laser slope efficiency. The use of fiber Bragg grating may lead to single-longitudinal-mode operation with this laser.

Funding

References

1. S. Taccheo, P. Laporta, S. Longhi, O. Svelto, and C. Svelto, "Diode-pumped bulk erbium–ytterbium lasers," Appl. Phys. B **63**(5), 425–436 (1996).
2. J. D. B. Bradley and M. Pollnau, "Erbium-doped integrated waveguide amplifiers and lasers," Laser Photonics Rev. **5**(3), 368–403 (2011).
3. R. Brinkmann, W. Sohler, and H. Suche, "Continuous-wave erbium-diffused $LiNbO_3$ waveguide laser," Electron. Lett. **27**(5), 415–417 (1991).
4. T. Feuchter, E. K. Mwarania, J. Wang, L. Reekie, and J. S. Wilkinson, "Erbium-doped ion-exchanged waveguide lasers in BK-7 glass," IEEE Photonics Technol. Lett. **4**(6), 542–544 (1992).
5. E. H. Bernhardi, H. A. G. M. van Wolferen, L. Agazzi, M. R. H. Khan, C. G. H. Roeloffzen, K. Wörhoff, M. Pollnau, and R. M. de Ridder, "Ultra-narrow-linewidth, single-frequency distributed feedback waveguide laser in $Al_2O_3:Er^{3+}$ on silicon," Opt. Lett. **35**(14), 2394–2396 (2010).
6. K.-M. Wang, B.-R. Shi, N. Cue, Y.-Y. Zhu, R.-F. Xiao, F. Lu, W. Li, and Y.-G. Liu, "Waveguide laser film in erbium-doped $KTiOPO_4$ by pulsed laser deposition," Appl. Phys. Lett. **73**(8), 1020–1022 (1998).
7. S. A. Vázquez-Córdova, S. Aravazhi, C. Grivas, Y.-S. Yong, S. M. García-Blanco, J. L. Herek, and M. Pollnau, "High optical gain in erbium-doped potassium double tungstate channel waveguide amplifiers," Opt. Express **26**(5), 6260–6266 (2018).
8. S. Taccheo, G. Della Valle, R. Osellame, G. Cerullo, N. Chiodo, P. Laporta, O. Svelto, A. Killi, U. Morgner, M. Lederer, and D. Kopf, "Er:Yb-doped waveguide laser fabricated by femtosecond laser pulses," Opt. Lett. **29**(22), 2626–2628 (2004).

9. F. Vetrone, J.-C. Boyer, J. A. Capobianco, A. Speghini, and M. Bettinelli, "Concentration-dependent near-infrared to visible upconversion in nanocrystalline and bulk Y_2O_3:Er^{3+}," Chem. Mater. **15**(14), 2737–2743 (2003).
10. F. Vetrone, J. C. Boyer, J. A. Capobianco, A. Speghini, and M. Bettinelli, "Effect of Yb^{3+} codoping on the upconversion emission in nanocrystalline Y_2O_3: Er^{3+}," J. Phys. Chem. B **107**(5), 1107–1112 (2003).
11. G. Karlsson, F. Laurell, J. Tellefsen, B. Denker, B. Galagan, V. Osiko, and S. Sverchkov, "Development and characterization of Yb-Er laser glass for high average power laser diode pumping," Appl. Phys. B **75**(1), 41–46 (2002).
12. S. Jiang, M. Myers, and N. Peyghambarian, "Er^{3+} doped phosphate glasses and lasers," J. Non-Cryst. Sol. **239**(1–3), 143–148 (1998).
13. J. W. Kim, D. Y. Shen, J. K. Sahu, and W. A. Clarkson, "High-power in-band pumped Er:YAG laser at 1617 nm," Opt. Express **16**(8), 5807–5812 (2008).
14. J. M. Serres, P. Loiko, V. Jambunathan, X. Mateos, V. Vitkin, A. Lucianetti, T. Mocek, M. Aguiló, F. Díaz, U. Griebner, and V. Petrov, "Efficient diode-pumped Er:KLu(WO$_4$)$_2$ laser at ~1.61 μm," Opt. Lett. **43**(2), 218–221 (2018).
15. V. Petrov, M. C. Pujol, X. Mateos, O. Silvestre, S. Rivier, M. Aguilo, R. M. Sole, J. Liu, U. Griebner, and F. Diaz, "Growth and properties of KLu(WO$_4$)$_2$, and novel ytterbium and thulium lasers based on this monoclinic crystalline host," Laser Photonics Rev. **1**(2), 179–212 (2007).
16. J. Liu, V. Petrov, X. Mateos, H. Zhang, and J. Wang, "Efficient high-power laser operation of Yb:KLu(WO$_4$)$_2$ crystals cut along the principal optical axes," Opt. Lett. **32**(14), 2016–2018 (2007).
17. J. M. Serres, X. Mateos, P. Loiko, K. Yumashev, N. Kuleshov, V. Petrov, U. Griebner, M. Aguiló, and F. Díaz, "Diode-pumped microchip Tm:KLu(WO$_4$)$_2$ laser with more than 3 W of output power," Opt. Lett. **39**(14), 4247–4250 (2014).
18. P. Loiko, J. M. Serres, X. Mateos, K. Yumashev, N. Kuleshov, V. Petrov, U. Griebner, M. Aguiló, and F. Díaz, "In-band-pumped Ho:KLu(WO$_4$)$_2$ microchip laser with 84% slope efficiency," Opt. Lett. **40**(3), 344–347 (2015).
19. D. Geskus, S. Aravazhi, K. Wörhoff, and M. Pollnau, "High-power, broadly tunable, and low-quantum-defect KGd$_{1-x}$Lu$_x$(WO$_4$)$_2$:Yb^{3+} channel waveguide lasers," Opt. Express **18**(25), 26107–26112 (2010).
20. K. van Dalfsen, S. Aravazhi, C. Grivas, S. M. García-Blanco, and M. Pollnau, "Thulium channel waveguide laser with 1.6 W of output power and ~80% slope efficiency," Opt. Lett. **39**(15), 4380–4383 (2014).
21. W. Bolaños, J. J. Carvajal, M. C. Pujol, X. Mateos, G. Lifante, M. Aguiló, and F. Díaz, "Epitaxial growth of lattice matched KY$_{1-x-y}$Gd$_x$Lu$_y$(WO$_4$)$_2$ thin films on KY(WO$_4$)$_2$ substrates for waveguiding applications," Cryst. Growth Des. **9**(8), 3525–3531 (2009).
22. N. V. Kuleshov, A. A. Lagatsky, V. G. Shcherbitsky, V. P. Mikhailov, E. Heumann, T. Jensen, A. Diening, and G. Huber, "CW laser performance of Yb and Er, Yb doped tungstates," Appl. Phys. B **64**(4), 409–413 (1997).
23. K. Gorbachenya, V. E. Kisel, S. V. Kurilchik, A. S. Yasukevich, S. Korableva, V. V. Semashko, A. A. Pavlyuk, and N. V. Kuleshov, "Er:KY(WO$_4$)$_2$ and Er:LiYF$_4$ crystals for eye-safe in-band pumped lasers," in *Advanced Solid State Lasers* (Optical Society of America, 2015), P. AM5A.14.
24. K. A. Subbotin, E. V. Zharikov, and V. A. Smirnov, "Yb- and Er-doped single crystals of double tungstates NaGd(WO$_4$)$_2$, NaLa(WO$_4$)$_2$, and NaBi(WO$_4$)$_2$ as active media for lasers operating in the 1.0 and 1.5 μm ranges," Opt. Spectrosc. **92**(4), 601–608 (2002).
25. W. Bolaños, J. J. Carvajal, X. Mateos, M. C. Pujol, N. Thilmann, V. Pasiskevicius, G. Lifante, M. Aguiló, and F. Díaz, "Epitaxial layers of KY$_{1-x-y}$Gd$_x$Lu$_y$(WO$_4$)$_2$ doped with Er^{3+} and Tm^{3+} for planar waveguide lasers," Opt. Mater. **32**(3), 469–474 (2010).
26. S. García-Revilla, R. Valiente, Y. E. Romanyuk, and M. Pollnau, "Temporal dynamics of upconversion luminescence in Er^{3+}, Yb^{3+} co-doped crystalline KY(WO$_4$)$_2$ thin films," J. Lumin. **128**(5–6), 934–936 (2008).
27. S. Kurilchik, O. Dernovich, K. Gorbachenya, V. Kisel, I. Kolesova, A. Kravtsov, S. Guretsky, and N. Kuleshov, "Growth, spectroscopy, and laser characterization of Er:KGd$_x$Yb$_y$Y$_{1-x-y}$(WO$_4$)$_2$ epitaxial layers," Opt. Lett. **42**(21), 4565–4568 (2017).
28. M. Ams, G. D. Marshall, P. Dekker, J. A. Piper, and M. J. Withford, "Ultrafast laser written active devices," Laser Photonics Rev. **3**(6), 535–544 (2009).
29. A. Okhrimchuk, "Femtosecond fabrication of waveguides in ion-doped laser crystals," in *Coherence and Ultrashort Pulse Laser Emission*, F. J. Duarte, Ed. (InTech, 2010), pp. 519–542.
30. F. Chen and J. R. Vázquez de Aldana, "Optical waveguides in crystalline dielectric materials produced by femtosecond-laser micromachining," Laser Photonics Rev. **8**(2), 251–275 (2014).
31. G. Della Valle, R. Osellame, N. Chiodo, S. Taccheo, G. Cerullo, P. Laporta, A. Killi, U. Morgner, M. Lederer, and D. Kopf, "C-band waveguide amplifier produced by femtosecond laser writing," Opt. Express **13**(16), 5976–5982 (2005).
32. R. Osellame, G. Della Valle, N. Chiodo, S. Taccheo, P. Laporta, O. Svelto, and G. Cerullo, "Lasing in femtosecond laser written optical waveguides," Appl. Phys., A Mater. Sci. Process. **93**(1), 17–26 (2008).
33. J. Hoyo, V. Berdejo, T. T. Fernandez, A. Ferrer, A. Ruiz, J. A. Valles, M. A. Rebolledo, I. Ortega-Feliu, and J. Solis, "Femtosecond laser written 16.5 mm long glass-waveguide amplifier and laser with 5.2 dB cm^{-1} internal gain at 1534 nm," Laser Phys. Lett. **10**(10), 105802 (2013).
34. F. M. Bain, A. A. Lagatsky, R. R. Thomson, N. D. Psaila, N. V. Kuleshov, A. K. Kar, W. Sibbett, and C. T. A. Brown, "Ultrafast laser inscribed Yb:KGd(WO$_4$)$_2$ and Yb:KY(WO$_4$)$_2$ channel waveguide lasers," Opt. Express **17**(25), 22417–22422 (2009).

35. E. Kifle, X. Mateos, J. R. de Aldana, A. Ródenas, P. Loiko, S. Y. Choi, F. Rotermund, U. Griebner, V. Petrov, M. Aguiló, and F. Díaz, "Femtosecond-laser-written Tm:KLu(WO$_4$)$_2$ waveguide lasers," Opt. Lett. **42**(6), 1169–1172 (2017).

36. E. Kifle, P. Loiko, X. Mateos, J. R. Vázquez de Aldana, A. Ródenas, U. Griebner, V. Petrov, M. Aguiló, and F. Díaz, "Femtosecond-laser-written hexagonal cladding waveguide in Tm:KLu(WO$_4$)$_2$: μ-Raman study and laser operation," Opt. Mater. Express **7**(12), 4258–4268 (2017).

37. P. Loiko, P. Segonds, P. L. Inácio, A. Peña, J. Debray, D. Rytz, V. Filippov, K. Yumashev, M. C. Pujol, X. Mateos, M. Aguiló, F. Díaz, M. Eichhorn, and B. Boulanger, "Refined orientation of the optical axes as a function of wavelength in three monoclinic double tungstate crystals KRE(WO$_4$)$_2$ (RE = Gd, Y or Lu)," Opt. Mater. Express **6**(9), 2984–2990 (2016).

38. A. Ródenas, G. A. Torchia, G. Lifante, E. Cantelar, J. Lamela, F. Jaque, L. Roso, and D. Jaque, "Refractive index change mechanisms in femtosecond laser written ceramic Nd:YAG waveguides: micro-spectroscopy experiments and beam propagation calculations," Appl. Phys. B **95**(1), 85–96 (2009).

39. A. Ródenas, A. H. Nejadmalayeri, D. Jaque, and P. Herman, "Confocal Raman imaging of optical waveguides in LiNbO$_3$ fabricated by ultrafast high-repetition rate laser-writing," Opt. Express **16**(18), 13979–13989 (2008).

40. S. M. Eaton, C. A. Merchant, R. Iyer, A. J. Zilkie, A. S. Helmy, J. S. Aitchison, P. R. Herman, D. Kraemer, R. J. D. Miller, C. Hnatovsky, and R. S. Taylor, "Raman gain from waveguides inscribed in KGd(WO$_4$)$_2$ by high repetition rate femtosecond laser," Appl. Phys. Lett. **92**(8), 081105 (2008).

41. H.-D. Nguyen, A. Ródenas, J. R. Vázquez de Aldana, J. Martínez, F. Chen, M. Aguiló, M. C. Pujol, and F. Díaz, "Heuristic modelling of laser written mid-infrared LiNbO$_3$ stressed-cladding waveguides," Opt. Express **24**(7), 7777–7791 (2016).

42. J. A. Caird, S. A. Payne, P. R. Staber, A. J. Ramponi, L. L. Chase, and W. F. Krupke, "Quantum electronic properties of the Na$_3$Ga$_2$Li$_3$F$_{12}$:Cr^{3+} laser," IEEE J. Quantum Electron. **24**(6), 1077–1099 (1988).

43. G. Della Valle, S. Taccheo, R. Osellame, A. Festa, G. Cerullo, and P. Laporta, "1.5 mum single longitudinal mode waveguide laser fabricated by femtosecond laser writing," Opt. Express **15**(6), 3190–3194 (2007).

44. N. D. Psaila, R. R. Thomson, H. T. Bookey, N. Chiodo, S. Shen, R. Osellame, G. Cerullo, A. Jha, and A. K. Kar, "Er:Yb-doped oxyfluoride silicate glass waveguide laser fabricated using ultrafast laser inscription," IEEE Photonics Technol. Lett. **20**(2), 126–128 (2008).

45. J. del Hoyo, P. Moreno-Zárate, G. Escalante, J. A. Vallés, P. Fernández, and J. Solís, "High-efficiency waveguide optical amplifiers and lasers via fs-laser induced local modification of the glass composition," J. Lightwave Technol. **35**(14), 2955–2959 (2017).

46. F. Moglia, S. Müller, F. Reichert, P. W. Metz, T. Calmano, C. Kränkel, E. Heumann, and G. Huber, "Efficient upconversion-pumped continuous wave Er^{3+}:LiLuF$_4$ lasers," Opt. Mater. **42**, 167–173 (2015).